A Time-Domain Computer Simulator of the Nonlinear Response of Semiconductor Optical Amplifiers

Dajana Cassioli, Simona Scotti, and Antonio Mecozzi, *Member, IEEE*

***Abstract*—We present a computer simulator of semiconductor optical amplifiers. The nonlinear input–output response of the device is characterized in terms of a complex gain, representing the accumulated gain and wavevector change of the propagating field across the active waveguide. We account for the gain saturation induced by stimulated recombination and by the perturbation of the carrier quasi-equilibrium distribution within the bands. A rigorous elimination of the spatial coordinate allows us to reduce the description of the amplifier dynamics to the solution of a set of ordinary differential equation for the complex gain. If the waveguide internal loss is negligible, the spatial inhomogeneity of the complex gain is implicitly yet exactly taken into account by the reduced model. The accuracy of the reduced model is the same for models based on the direct solution of the set of partial differential equations describing the interaction between the optical field and the active semiconductor waveguide, but the model is computationally much simpler. To preserve the input–output characteristics of the model, we include the amplified spontaneous emission noise in the device description by an equivalent signal applied to the device input and amplified by the saturated gain. At the expense of a minor increase of the program complexity, the waveguide internal loss may also be included. We report on the comparison between the output of the simulator and the results of four-wave mixing experiments in various pump-signal configurations. Good agreement is obtained.**

***Index Terms*—Modeling, optical communication, optical mixing, optical propagation in nonlinear media, semiconductor optical amplifiers, simulation software.**

I. Introduction

In RECENT years, the market penetration of electronic computers and the continuous increase of computational speed produced a rapid growth of the service demand for data communications, leading to the expectation of a high growth rate in telecommunication traffic over the next few years [1]. The large expansion of the telecommunication market requires a more organized and flexible evolution of the network infrastructures. The realization of a new generation of optical networks able to manage high-speed data flows is therefore needed [2], [3]. Optical amplifiers are an important part of high-speed optical networks. Although semiconductor optical amplifiers (SOAs) were proposed first, the high optical linearity of the erbium-doped fiber amplifier (EDFA) [4] is the main reason for its widespread penetration as an in-line repeater in high-speed optical links. Optical linearity also makes these devices ideal for wavelength-division multiplexing (WDM), making nonlinear crosstalk between WDM channels virtually nonexistent. The use of SOAs has therefore been envisaged in different applications, both in local-area networks for their potential low cost and for signal processing because of their high speed and optical nonlinearity. In the linear regime, the SOA fast response to bias current variations makes it an efficient electrically controlled fast switch to be employed in optical gates [5], [6]. In the nonlinear regime, SOAs may be used in a variety of different applications as devices for all-optical signal processing [7]–[9]. Because the main characteristic of SOAs is their high nonlinearity, the analysis and the evaluation of the SOA performance for virtually any application must necessarily be made taking into account all the relevant optical nonlinearities of the device. For SOA repeaters, the analysis of the optical nonlinearities is important to find the limits of the linear operation range. In this context, efficient computer simulators are very useful for the optimization of the device operating conditions and for the evaluation of the performance of a complete optical communication system. For SOA-based photonic devices, efficient simulators are obviously even more useful at the design stage and for performance analysis.

In this paper, we describe a computer simulator of SOAs based on the theoretical model reported in [10]. The theory includes the physical processes that characterize the approach to quasi-equilibrium of the carrier distribution perturbed by stimulated recombination, namely, spectral hole burning (SHB) and carrier heating (CH), as well as interband processes. The characteristic time of these processes ranges from 50 fs to 100 ps [11], [12]. The peculiarity of this simulator is that the analysis is made by solving a differential equation in time, never calling for the use of the fast Fourier transform (FFT) algorithm in the solution of the SOA dynamic equations. This way, the program automatically meets causality, since the output waveform depends on the input at previous times only. This property makes our simulator different from those based on the FFT that, because of the periodic boundary conditions implied by the algorithm, require prior knowledge of the complete input waveform over the whole time window considered by the simulation.

Let us now summarize the contents of this paper. We will first briefly review the theoretical model, then we will describe the numerical model based on this theory and its use in a computer simulator implemented in Simulink, a package of Matlab. Finally, we will compare the simulations with experimental results. Although we will mainly concentrate on four-wave mixing (FWM) experiments, for which we have available experimental results to compare, our model is indeed more general, and it may be used to simulate SOAs used

Manuscript received September 2, 1999; revised May 10, 2000. This work was supported in part by the European Project COST 267.

D. Cassioli is with the Dipartimento di Ingegneria Elettronica, II Università degli Studi di Roma "Tor Vergata," 00133 Rome, Italy.

S. Scotti is with Fondazione Ugo Bordoni, 00142 Rome, Italy.

A. Mecozzi is with the Istituto Nazionale di Fisica della Materia and Dipartimento di Ingegneria Elettrica, Università… degli Studi dell'Aquila, 67040 Poggio di Roio, L'Aquila, Italy.

Publisher Item Identifier S 0018-9197(00)07268-7.

both in linear transmission experiments and in cross-gain and cross-phase modulation converters.

II. Theoretical Model

The nonlinear interaction between the optical field and the active medium takes place during propagation and amplification (or attenuation) of the field along the semiconductor waveguide. The dynamics of the intensity and phase of the field therefore depend on both time and the longitudinal coordinate (i.e., the propagation axis of the waveguide), and a complete characterization of the evolution of the propagating field within the SOA is intrinsically a two-dimensional (2-D) problem.

Many numerical models of SOAs describe the temporal evolution of the field during propagation and calculate the optical field at the device output by numerically solving a set of partial differential equations. In such numerical models, the waveguide is partitioned into regions in which the physical properties of the medium are approximately constant. A dense partition for a given waveguide length usually guarantees a high accuracy of the results, obviously obtained at the expense of long computation times.

In the model proposed in [10], an exact analytical integration along the longitudinal coordinate (z) over the entire device length permits one to reduce the 2-D problem to a set of ordinary differential equations (ODE) in which time is the only independent variable. With this procedure, the SOA is described by its impulse response, which is rigorously calculated including both the longitudinal variation and the temporal evolution of the field, yet avoiding the need to explicitly calculate the field inside the device. The reduction of the device description to its input–output relation makes our model particularly suited for use in modular simulation tools designed to describe the response of an optical system to a given arbitrary input waveform.

Let us briefly summarize how the initial set of partial differential equations has been reduced to a set of ODEs. At the deepest level, the nonlinear interaction between the propagating field and the semiconductor material produces local changes of the carrier density distribution along the propagation direction. Nonlinear processes, such as SHB and CH, characterizing the approach to quasi-equilibrium of the carrier distribution initially perturbed by the interaction with the optical field, induce such changes. The starting set of differential equations is therefore based on a microscopic model of the semiconductor that describes the carrier density dynamics, including carrier density depletion (CDD), CH, and SHB [12], [13]. Nonlinear processes with characteristic times shorter than SHB (such as two-photon absorption or the Kerr effect [14], [15]) are not considered in the model because their effect is not significant unless picosecond and subpicosecond pulses are used.

In this microscopic approach, the total variation of the carrier distribution at a general position z within the waveguide is expressed as a combination of the different "local density" changes, $\Delta n_{\rm CDD}$, $\Delta n_{\rm CH}$, and $\Delta n_{\rm SHB}$, associated with these physical processes. Because the gain and the refractive index of the semiconductor depend on these local densities, each local density distribution is associated with a distinct term that contributes to the total gain. The gain may be expanded as the sum of three contributions due to different processes: the first, g_l, related to carrier density depletion and the other two, $g_{\rm CH}$ and $g_{\rm SHB}$, due to ultrafast nonlinear processes. The set of differential equations that describes the active semiconductor consists of rate equations for the variables g_i ($i = l$, CH, SHB). In [10], separate sets of equations were considered for the conduction and valence band; in this paper, as commonly accepted, we neglect the hole dynamics and consider only electrons because of their smaller effective mass and, hence, longer relaxation time.

The three rate equations describing the temporal evolution of the three quantities g_i depend on the photon density profile and are therefore coupled to the equation that describes the propagation of the field along the waveguide. The inclusion of the propagation equation for the field in the analytical description makes this model 2-D, since it is described by a set of partial differential equations on the independent variables t (time) and z (longitudinal coordinate). The key to reducing this problem to a one-dimensional (1-D) problem is the integration of both sides of the partial differential equations over the entire device length. This leads to a new set of differential equations in the three variables h_j defined as the contribution of each process to the integrated gain coefficient (g_m) of the device, $h_j(t) = \Gamma \int_0^L dz' g_j(t, z)$ with $j = N$, CH, SHB. The coefficient Γ is the mode confinement factor, whereas h_N, $h_{\rm CH}$, and $h_{\rm SHB}$ are the contributions to the overall gain of CDD, CH, and SHB, respectively. Using the definition of h_j, we obtain for the integrated gain coefficient

$$g_m(t) = \Gamma \int_0^L dz' g(t, z') \equiv h_N(t) + h_{\rm SHB}(t) + h_{\rm CH}(t). \quad (1)$$

The overall gain of the device is therefore given by the expression

$$G(t) = \exp[g_m(t)] \equiv \exp[h_N + h_{\rm CH} + h_{\rm SHB}]. \quad (2)$$

The initial set is thus reduced to the following ordinary differential equations for the new variables h_j:

$$\frac{dh_N}{dt} = -\frac{h_N}{\tau_S} - \frac{1}{P_S \tau_S}[G(t) - 1]P_{\rm in}(t) + \frac{g_0}{\tau_S} \quad (3a)$$

$$\frac{dh_{\rm SHB}}{dt} = -\frac{h_{\rm SHB}}{\tau_1} - \frac{\varepsilon_{\rm SHB}}{\tau_1}[G(t) - 1]P_{\rm in}(t) - \frac{dh_{\rm CH}}{dt} - \frac{dh_N}{dt} \quad (3b)$$

$$\frac{dh_{\rm CH}}{dt} = -\frac{h_{\rm CH}}{\tau_h} - \frac{\varepsilon_{\rm CH}}{\tau_h}[G(t) - 1]P_{\rm in}(t). \quad (3c)$$

Here, g_0 is the unsaturated gain of the device, τ_1 is the carrier–carrier scattering time, τ_h is the temperature relaxation time, τ_S is the carrier lifetime, and $P_{\rm in}$ is the optical power at the SOA input. The other parameters are the nonlinear gain suppression factors due to CH and SHB $\varepsilon_{\rm CH}$ and $\varepsilon_{\rm SHB}$ and the saturation power P_S.

Because of the Kramers–Kronig relations, any change in the optical gain affects the waveguide refractive index. To first order, the phase $\phi(t)$ of the optical field at output, which depends on the index, may be expressed as a linear function of the same variables describing the optical gain as

$$\phi(t) = -\frac{1}{2}\alpha_N[h_N - g_o] - \frac{1}{2}\alpha_T h_{\rm CH} \quad (4)$$

where α_N and α_T are the phase-amplitude coupling coefficients of carrier density pulsation and carrier heating, respectively.

The set of rate equations (3) for the variables h_j, along with (1) and (4), shows that the input field power $P_{\rm in}(t)$ is the only excitation function of the system. Once the rate equations (3) are solved for a given $P_{\rm in}(t)$, (1) gives the overall power gain of the device and (4) gives the overall phase variation that the input field experiences through propagation along the semiconductor waveguide. Thus, the output field $E_{\rm out}(t)$ may be calculated by applying the amplitude gain $G(t)^{1/2}$ and the phase $\phi(t)$ to the input field $E_{\rm in}(t)$, that is,

$$E_{\rm out}(t) = E_{\rm in}(t) \cdot e^{\{(1/2)g_m(P_{\rm in}(t))+i\phi(P_{\rm in}(t))\}}. \tag{5}$$

Note that, although the parameters α_N and α_T do not compare in the set of ODEs (3) and therefore do not affect the total output power of the device, they affect the phase of the output field and therefore its spectrum. These parameters will be essential in determining the FWM efficiency, since the output field within a given frequency range strongly depends on the overall phase of the output field.

The solution of the ODE set gives the field at the output of an *ideal* device. The description of a *real* device requires the inclusion of two more processes, amplified spontaneous emission (ASE) and waveguide internal loss. We will describe in the next section how to include ASE noise in the SOA model while preserving its input–output characteristics. We will also show how propagation losses can be taken into account in the section devoted to the description of the simulator.

III. ASE Noise

One of the main processes to consider in the SOA analysis is ASE noise, because it strongly affects the device performance. To preserve the input–output character of the theoretical model [10], we looked for ways to simulate the ASE noise by an equivalent noise source with appropriate statistical properties. The goal is to inject the noise at the device input like any other signal (pump or modulated signal).

Neglecting internal loss, the field propagating inside the active waveguide in the presence of ASE noise obeys the propagation equation

$$\frac{dE(t,\,z)}{dz} = \left[\frac{1}{2}\Gamma g(t,\,z) + i\phi(t,\,z)\right] E(t,\,z) + [\hbar\omega_0 n_{sp} g(t,\,z)]^{1/2}\, n(t,\,z). \tag{6}$$

The complex term $n(t,\,z)$ is the ASE noise contribution, which we model as a Gaussian phase-independent spatially uncorrelated white noise process. This is equivalent to assuming the average and autocorrelation functions

$$\langle n(t,\,z)\rangle = \langle n(t_1,\,z_1)n(t_2,\,z_2)\rangle = 0 \tag{7a}$$

$$\langle n(t_1,\,z_1)n^*(t_2,\,z_2)\rangle = \delta(t_1 - t_2)\delta(z_1 - z_2). \tag{7b}$$

The $n(t,\,z)$ process defined in (7) has infinite bandwidth and, hence, infinite power. In the real world, the finite spectral width of the gain spectrum gives a finite bandwidth to the noise as well. Since we do not consider the frequency dependency of the gain in our model, we need to use a band-limited noise, and we accomplish this goal by, instead of using $n(t,\,z)$, using the process obtained by filtering $n(t,\,z)$ through a bandpass filter with a frequency response $F(\Omega)$. The width of $F(\Omega)$ will be chosen to be comparable with the gain bandwidth. The filtered ASE noise is described in the time domain by

$$N(t,\,z) = \int_{-\infty}^{\infty} f(t - t')n(t',\,z)\,dt' \tag{8}$$

where the impulse response $f(t)$ is the inverse Fourier transform of $F(\Omega)$, meeting the causality condition $f(t) = 0$ for $t < 0$. The average and autocorrelation functions of the band-limited noise are

$$\langle N(t,\,z)\rangle = \langle N(t_1,\,z_1)N(t_2,\,z_2)\rangle = 0 \tag{9a}$$

$$\langle N(t_1,\,z_1)N^*(t_2,\,z_2)\rangle = \left[\int_{-\infty}^{\infty} f(\tau)f^*(\tau + \Delta t)\,d\tau\right] \cdot \delta(z_1 - z_2), \tag{9b}$$

where $\Delta t = t_2 - t_1$ and we used (7) and (8) in (9b). With filtered noise, (6) becomes

$$\frac{dE(t,\,z)}{dz} = \left[\tfrac{1}{2}\Gamma g(t,\,z) + i\phi(t,\,z)\right] E(t,\,z) + [\hbar\omega_0 n_{\rm sp} g(t,\,z)]^{1/2} N(t,\,z). \tag{10}$$

We assume that the spontaneous emission coefficient $n_{\rm sp}$ is independent of saturation, a good approximation for devices operating at moderate saturation levels. The solution of (10) is therefore

$$E(t,\,z) = E_{\rm in}(t)\exp\left\{\int_0^z dz''\left[\frac{\Gamma}{2}g(t,\,z'') + i\phi(t,\,z'')\right]\right\} + \int_0^z dz'[\hbar\omega_0 n_{sp} g(t,\,z')]^{1/2} N(t,\,z') \cdot \exp\left\{\int_{z'}^z dz''\left[\frac{\Gamma}{2}g(t,\,z'') + i\phi(t,\,z'')\right]\right\}. \tag{11}$$

Equation (11) gives the output field at the longitudinal coordinate z due to the input signal and to the ASE noise generated inside the device. This expression will be used to define the equivalent noise source to be added at the input of the ideal noiseless device. The definition of an equivalent noise source is common practice in electronics to describe noisy electric circuits. We first notice that (11) can be written at $z = L$ as

$$E(t,\,L) = [E_{\rm in}(t) + E_{\rm ASE}(t,\,L)] \cdot \exp\left\{\int_0^L dz'\left[\frac{\Gamma}{2}g(t,\,z') + i\phi(t,\,z')\right]\right\} \tag{12}$$

where

$$E_{\rm ASE}(t,\,L) = \int_0^L [\hbar\omega_o n_{sp} g(t,\,z')]^{1/2} N'(t,\,z') \cdot \exp\left[-\int_0^{z'} dz''\frac{\Gamma}{2}g(t,\,z'')\right] dz' \tag{13}$$

and

$$N'(t,\,z) = N(t,\,z)\exp\left[-i\int_0^z \phi(t,\,z'')\,dz'\right]. \tag{14}$$

The transformed noise term $N'(t, z)$ is statistically equivalent to $N(t, z)$, because the autocorrelation functions are the same for both processes. Equation (12) gives the optical field at the device output ($z = L$) as a function of the input field $E_{\rm in}(t)$. The stochastic process $E_{\rm ASE}(t, L)$ is obtained by adding the contribution for all z of the noise generated at z divided by the gain that the field experiences from the input to z.

Let us now evaluate the statistical properties of the process $E_{\rm ASE}(t, L)$. We have

$$\langle E_{\rm ASE}(t, L)\rangle = \langle E_{\rm ASE}(t, L)E_{\rm ASE}(t+\Delta t, L)\rangle = 0. \quad (15)$$

The evaluation of $\langle E_{\rm ASE}(t, L)E^*_{\rm ASE}(t+\Delta t, L)\rangle$ requires a little algebra and some additional approximations. Using (9b), (13), and (14), we obtain

$$\begin{aligned}&\langle E_{\rm ASE}(t, L)E^*_{\rm ASE}(t+\Delta t, L)\rangle\\ &\quad = \hbar\omega_0 n_{\rm sp}\int_{-\infty}^{\infty} f(\tau)f^*(\tau+\Delta t)\,d\tau\int_0^L dz'\\ &\qquad \cdot [g(t, z')g(t+\Delta t, z')]^{1/2}\\ &\qquad \cdot \exp\left\{-\int_0^{z'} dz_1\frac{\Gamma}{2}[g(t, z_1)+g(t+\Delta t, z_1)]\right\} dz. \quad (16)\end{aligned}$$

The integral in τ is a sharply peaked function of Δt having a width of the order of the inverse of the noise bandwidth. Over this time interval, in the femtosecond range, we may assume $g(t, z_1) \cup g(t+\Delta t, z_1)$, and approximate (16) as

$$\begin{aligned}&\langle E_{\rm ASE}(t, L)E^*_{\rm ASE}(t+\Delta t, L)\rangle \approx\\ &\quad = \hbar\omega_0 n_{\rm sp}\int_{-\infty}^{\infty} f(\tau)f^*(\tau+\Delta t)\,d\tau\int_0^L dz' g(t, z')\\ &\qquad \cdot \exp\left\{-\int_0^{z'} dz_1\Gamma g(t, z_1)\right\}. \quad (17)\end{aligned}$$

Performing the integral, we finally obtain

$$\begin{aligned}&\langle E_{\rm ASE}(t, L)E^*_{\rm ASE}(t+\Delta t, L)\rangle\\ &\quad = \hbar\omega_0 n_{\rm sp}\int_{-\infty}^{\infty} f(\tau)f^*(\tau+\Delta t)\,d\tau\{1-\exp[-g_m(t, L)]\}\end{aligned} \quad (18)$$

If condition $g_m(t, L) >> 1$ is met, we may neglect the exponential function into the braces and the autocorrelation functions become independent of both the device length L and the gain. The process $E_{\rm ASE}(t, L)$ can therefore be well approximated by a complex phase-independent Gaussian variable, independent of the saturated gain $g_m(t, L)$ and length L, $E_{\rm ASE}(t, L) \cong E_{\rm ASE}(t)$. Using this approximation, the average and autocorrelation functions of the equivalent noise source becomes

$$\langle E_{\rm ASE}(t)\rangle = \langle E_{\rm ASE}(t)E_{\rm ASE}(t+\Delta t)\rangle = 0 \quad (19a)$$

$$\begin{aligned}R_{\rm ASE}(\Delta t) &= \langle E_{\rm ASE}(t)E^*_{\rm ASE}(t+\Delta t)\rangle\\ &= \hbar\omega_0 n_{\rm sp}\int_{-\infty}^{\infty} f(t)f^*(t+\Delta t)\,dt\end{aligned} \quad (19b)$$

and (12) becomes

$$\begin{aligned}E(t, z) = &[E_{\rm in}(t)+E_{\rm ASE}(t)]\\ &\cdot\exp\left\{\int_0^z dz'\left[\frac{\Gamma}{2}g(t, z')+i\phi(t, z')\right]\right\}.\end{aligned} \quad (20)$$

By integrating the square modulus of both members of (20) over z, we obtain the total power at the amplifier output, including the contribution of the ASE noise, as

$$\int_0^L dz'\Gamma g(t, z')|E(t, z')|^2 = [G(t)-1]P_{\rm in}(t) \quad (21)$$

where

$$P_{\rm in}(t) = |E_{\rm in}(t)+E_{\rm ASE}(t)|^2. \quad (22)$$

The previous analysis enables the theory of [10] to model the more general case in which ASE noise is included. Nevertheless, that theory neglects the counterpropagating ASE that contributes by approximately half of the saturation induced by the total ASE, and, therefore, this model of ASE noise is applicable only when the saturation induced by the noise itself is negligible compared to that induced by the input signal. When this condition is met, the model gives a practical and accurate description of device behavior in the presence of ASE noise. With our approach, a *noisy device* is represented as the cascade of an *equivalent noise source* (at the device input) which adds to the input signal [see (22)] and an *ideal, noiseless, device* described by the set of ODEs (3).

IV. Computer Model

For the implementation of the SOA simulator, we have chosen the Simulink software mainly because of its capacity to perform a time-domain analysis of dynamical systems. Simulink is based on the Matlab engine and routines for numerical calculations. A peculiarity of Simulink is the graphical user interface that allows the design of simulation models of dynamical systems by simply drawing a block-diagram on the computer monitor. One difficulty in using Simulink is related to the fact that usually optical devices are described in the frequency domain and their time-domain description is often more involved. As an example, some of the approximations commonly made in the frequency domain (e.g., the approximation of fiber dispersion as a phase-only filter) make noncausal the corresponding time-domain equations.

A further difficulty in simulating optical systems is the extremely high frequency of optical carrier signals requiring a small sampling period in a discrete time-domain representation. This is why, in the optical system simulation, we resorted to a base-band representation of optical signals. As an example, if we want to simulate the transmission of a modulated signal, we shift the signal spectrum by an amount ν_m equal to the carrier frequency of the signal spectrum.

In the Simulink environment, the simulation models are built in a hierarchical fashion. At the top we find a global scheme, i.e., the sketch of the whole system that the user draws on the monitor. This is built from subsystems, called "blocks," that in general represent basic system component (sources, transmission channel, optical device, receiver , etc.). A procedure called

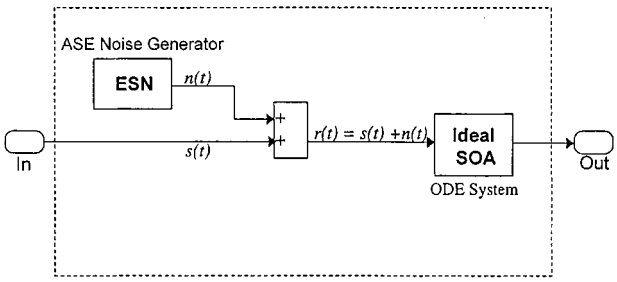

Fig. 1. Block scheme of the complete subsystem that represents the SOA.

"block masking" allows the user to associate a mask with each block. In the mask, the user defines an icon identifying the block and a list of characteristic parameters for the block. Parameters defined in the mask can be easily changed before running the simulation, or even while the simulation runs. The blocks can be built by assembling existing library blocks or by writing system functions (S-functions) in the Matlab language. Block nesting is possible and greatly useful. When the simulation is running, the engine solves the numerical solution of the underlying block models, and the user has access to the block output values at each integration step.

The SOA simulator is a typical subsystem and it is realized, as shown in Fig. 1, by assembling two blocks. One, identified by the icon "ideal SOA," describes the ODE system of (3) by an S-function. The other, labeled "ESN" in Fig. 1, represents the *equivalent source of* ASE *noise* generated within the semiconductor waveguide and it is modeled, as detailed above, as a source noise $n(t)$ injected at the device input. To ensure modularity, the two blocks exchange data only through signals traveling on the wires connecting them. The optical signal $s(t)$ is injected into the SOA at the input port (In) as a complex signal. Since Simulink only handles real signals, we divide the signal into its real and imaginary parts and represent it as a 2-D real vector.

The validity of the model and the values of the parameters used in the simulations were extensively tested by comparisons with experimental results. We mainly focused on FWM in SOAs for frequency conversion. We compared the FWM experiments with a CW pump and signal in which either a single pump [16] or two pumps [17], [18] are used. In the first case, the pump (at frequency ν_p) and the signal (ν_s) are injected into the device with the same polarization. The converted field is generated at frequency $\nu_c = \nu_p + \Omega$ (where Ω is the pump-signal detuning defined by $\nu_p - \nu_s$) [16], [19], [20]. We found it convenient to shift the signal spectrum by $-\nu_p$ and thus the pump appears at zero frequency and the signal at frequency Ω in the spectrum of the SOA input. In the second case, three optical fields are injected into the device, two pumps at frequency ν_{p1} and ν_{p2}, and a signal at frequency ν_s. The two pumps may have either parallel or orthogonal polarization. In this case, the frequency of one of the two pumps is chosen as the reference frequency for the injected signals.

A. Ideal SOA Block

The "ideal SOA" block has been made by writing an S-function that describes the ODE system (3). In the mask block are listed the parameters related to the optical nonlinearity of the device, namely the saturation power P_s, the nonlinear coefficients (ε_i), and the characteristic times of the nonlinear processes (τ_i), along with the small-signal gain $G_o = \exp(g_o)$, which depends on the current injected into the device. The initial value of the variable h_N is obtained by an external Matlab routine that extracts the steady-state solution of the ODEs with a CW input equal to the sum of all the field injected into the device. This procedure allows us to significantly reduce the initial transients of the simulations, which would otherwise require a few hundred picoseconds of simulation time to "thermalize."

TABLE I
DEVICE PARAMETERS USED IN THE SIMULATIONS

SEMICONDUCTOR OPTICAL AMPLIFIER
MASK

Small-signal gain	26	dB
Saturation power [W]	$10.8\ 10^{-3}$	W
Total spontaneous lifetime	70	ps
Spectral hole burning time	120	fs
Carrier heating time	480	fs
Gain compression coefficient for carrier heating ε_{CH}	1.95	W^{-1}
Gain compression coefficient for spectral burning ε_{SHB}	1.17	W^{-1}
Henry factor α_N	1.55	–
α_T factor	0.94	–

The results of all simulations reported in this paper are obtained with the parameters listed in Table I. The values of G_0 and P_s were obtained by a characterization of the device (500 μm long) used in the experiment of [16]. The values of the nonlinear coefficients were determined by a best fit of the theoretical curve of the conversion efficiency with experimental data [19], [21].

B. ASE Noise Generator

This block implements the *equivalent source of noise* (ESN) injected at the input of the ideal device to account for the ASE noise generated within the active waveguide. The noise field generated, $E_{\mathrm{ASE}}(t)$, is a band-limited complex white noise. We assume that the power spectral density of the ASE noise is constant in the band of interest, i.e., $\mathcal{P} = \hbar\omega_0 n_{sp}$. Thus, the power of the input noise is given by

$$P_{\mathrm{ASE}} = \int_{-\infty}^{+\infty} \hbar\omega_0 n_{\mathrm{sp}} |F(\Omega)|^2 \frac{d\Omega}{2\pi} = \hbar\omega_0 n_{\mathrm{sp}} B_N \qquad (23)$$

where

$$B_N = \int_{-\infty}^{+\infty} |F(\Omega)|^2 \frac{d\Omega}{2\pi}$$

is the noise equivalent bandwidth. The power density of a white-noise zero mean process is equal to its variance [$\mathcal{P} \equiv \sigma^2_{\mathrm{ASE}} = R_{\mathrm{ASE}}(0)$]. The noise field was expanded in terms of its real and imaginary parts $E_{\mathrm{ASE}}(t) = n_{\mathrm{re}}(t) + i n_{\mathrm{im}}(t)$, where the random processes $n_{\mathrm{re}}(t)$ and $n_{\mathrm{im}}(t)$ have equal variance, $\sigma^2_{\mathrm{re}} = \sigma^2_{\mathrm{im}} \equiv \sigma^2_{\mathrm{ASE}}/2 = \hbar\omega_o n_{\mathrm{sp}}/2$. The ESN block was built using two band-limited white Gaussian noise (BLWG) sources. In

the Simulink library, a generator is available supplying pseudorandom normally distributed numbers $\{x_i\}$ with zero mean and unit variance. The average power of an N-length sequence is given by

$$\frac{1}{N}\sum_{i=1}^{N}\langle x_i^2\rangle = 1.$$

The numbers $\{x_i\}$ should therefore be multiplied by $\sqrt{(\mathcal{P}/2)B_N}$ to approximate samples of the desired BLWG noise. Sampling theorem dictates that a sampling period $t_s \leq 1/2B_N$ must be used in the simulations. The output of the ESN block is the output of two BLWG blocks assembled to give a two-element vector $n(t)$.

The parameters in the mask of the ASE-noise generator subsystem are the optical carrier wavelength ω_o, the equivalent noise bandwidth B_N, and the spontaneous emission factor $n_{\rm sp}$. According to the theory, B_N should be comparable to the gain bandwidth. However, using a smaller noise equivalent bandwidth, sufficiently large to include all frequency components of the input signal, leads to a reduction in the computation time. It should be checked on a case-by-case basis that the value of the bandwidth used does not make the total ASE power large enough to give a significant contribution to the SOA saturation. As we mentioned above, our model cannot consistently consider the case of saturation by ASE, as we implicitly neglect the saturation induced by the counterpropagating ASE.

In our simulations, we determined the values assigned to the ASE noise generator parameters through a preliminary calibration procedure using noise data collected in FWM experiments. The spontaneous emission factor was adjusted to obtain the same noise power measured over the converted signal bandwidth. We made the noise calibration by using FWM data in the orthogonal two-pump configuration [17]. For the noise measurements, the converted signal was extracted at the device output by a monochromator of 5.6-GHz bandwidth. In this experiment, the input signal was switched off, leaving at the device input only the CW pumps. The power spectral density of the output noise was integrated over the 5.6-GHz bandwidth of the monochromator centered on the frequency at which the conjugate signal (C2) appears when the signal is switched on. Fig. 2 shows experimental results of ASE power in milliwatts as a function of the detuning between the pumps (P1,P2).

As shown in Fig. 2, the ASE power decreases at frequencies larger than 500 GHz because of the dispersion of the linear gain. Our simulator does not, however, include gain dispersion. This poses some limits to the maximum frequency detuning that can be considered. For calibration, we therefore fitted the ASE power spectral density at a detuning less than 500 GHz.

To reproduce the experimental setup, the field generated by the ESN block is coupled with the two pump fields. This total field is injected into the *ideal* SOA block. A filter, with a bandwidth of 5.6 GHz and centered at the C2 frequency, selects the signal at the output of the "ideal SOA" block. The signal energy is obtained by integrating the output signal over the run time T, and the value of the output power is calculated by the energy divided by T. The bandwidth B_N in the ESN mask was set to

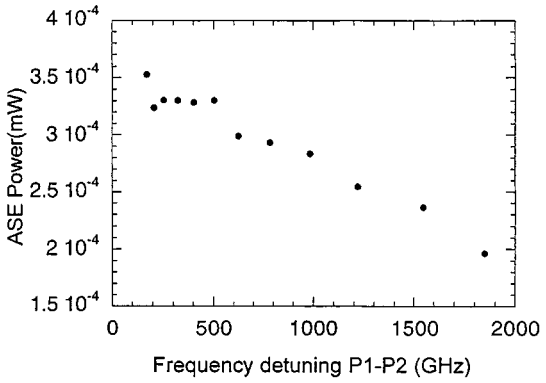

Fig. 2. Noise power measured in an SOA when two pumps, with orthogonal polarizations, are injected into the amplifier versus the detuning between the two pumps. The noise power is measured over a bandwidth of 5.6 GHz centered at a frequency detuned by 120 GHz to the frequency of the second pump.

1 THz, larger than the spectrum of the total input signal. With $n_{\rm sp} = 1$, we obtained about 0.3 μW of total noise power, in satisfactory agreement with the experimental data of Fig. 2.

C. Internal Loss

Although the theoretical approach described above does not include the SOA internal loss, these may be included in the SOA simulator without a significant addition to the complexity of the program. A first approach to the problem is reported in [10], where an approximate analytical solution is derived including the effects of internal loss. The theory of [10], however, although useful for extracting some qualitative understanding of the SOA dynamics with loss, is not easily implemented in a numerical simulation, because its final result is an integral equation whose numerical solution is cumbersome. We will use here an approach that is better adapted to the numerical solution of the problem.

With internal loss, the expression for the saturated gain (1) becomes

$$g_m(t) = \int_0^L dz[\Gamma g(t,z) - \alpha_{\rm int}] \tag{24}$$

where $\alpha_{\rm int}$ is the internal loss coefficient. Let us consider a device of length L and divide the propagation into M segments of length Δz. The internal loss is simulated by inserting linear attenuators of loss $A_{\Delta z} = \exp(-\alpha_{\rm int}\Delta z)$ between the segments. The behavior of each segment is then simulated as a single amplifier of length Δz with a small-signal gain $G_0^{1/M}$. We needed to optimize the number of cascaded amplifiers to obtain a good approximation of the device behavior in a small configuration time. The optimization was made by comparing the small-signal FWM response in the configuration with two copolarized pumps for a 500-μm amplifier in the cases in which the amplifier is described by 3 or 30 elements. The small-signal FWM response of a cascade of amplifiers was evaluated analytically using the theory of [10]. In Fig. 3, the result obtained with $M = 3$ is denoted by a dashed line, whereas those obtained with $M = 30$ are indicated by a solid line. It is evident that, for the case considered, three sections are already sufficient to characterize the device with an excellent accuracy.

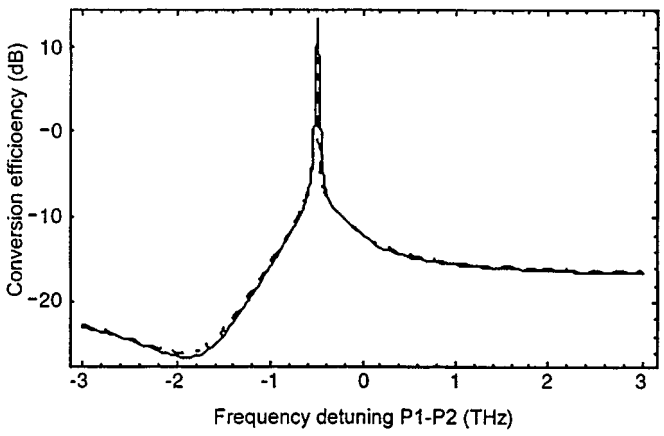

Fig. 3. Conversion efficiency obtained approximating the continuous loss of an SOA with lumped loss. The solid curve is obtained with 30 sections, the dashed curve with 3 sections.

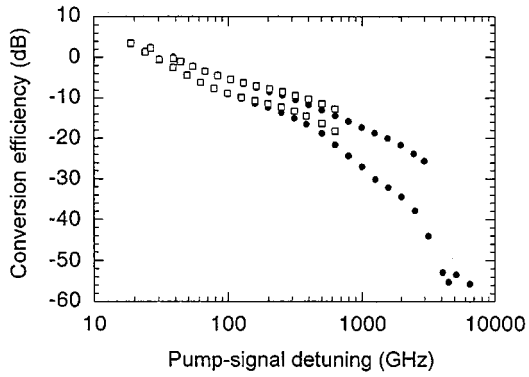

Fig. 4. Conversion efficiency versus pump-signal detuning in a configuration using a single pump. Dots represent experimental results, and squares represent the results of the simulation.

V. Comparison With the Experiment

In this section, we will compare with experiment the results of some simulations performed with our program. Although we will concentrate on FWM experiments, the simulator is capable of describing SOAs in more general environments. In particular, it may be used to simulate SOAs in transmission experiments and to analyze the combined effect of inter-symbol interference and inter-channel crosstalk in WDM transmission with SOAs [22], [23]. Another important application that we may envisage is the simulation of cross-gain modulation and, especially, interferometric cross-phase modulation converters. It has been shown that the chirp of the converted signal is a parameter significantly affecting the transmission performance of signals processed by interferometric converters. Our numerical model is able to accurately predict the chirp added to the output field by carrier depletion and by the ultrafast saturation processes and is, therefore, very useful for the investigation of the performance of these devices.

We simulated experiments of FWM in various configurations, either with a single or multiple pumps. We also evaluated the performance of an FWM converter, estimating the degradation of the transmission quality caused by ASE noise by extracting the bit error rate (BER) from a simulated eye diagram, using an approximate statistical procedure.

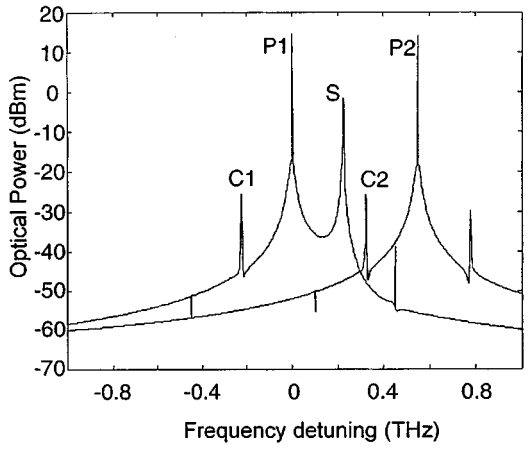

(a)

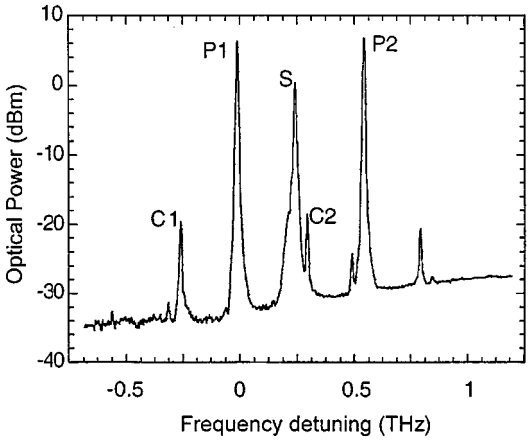

(b)

Fig. 5. (a) Simulated and (b) experimental spectra at the SOA output. A CW pump and a signal with the same polarization were injected at the SOA input, along with a second CW pump of orthogonal polarization.

A. Pump–Signal Scheme

In Fig. 4, we report the efficiency of frequency conversion versus the pump–signal frequency detuning. Dots represent the results of an FWM experiment with a single CW pump [16], and squares represent the results of the simulations. Good agreement is shown up to 0.7 THz in both up- and down-conversion. At higher frequency detuning where the processes of two-photon absorption and the Kerr effect (not included in our model) become relevant, the agreement becomes poorer. One should notice, however, that devices based on FWM operate at detuning smaller than 1 THz because of the extremely low efficiency at higher detunings. The poor accuracy at detunings higher than 1 THz, therefore, does not limit the use of the numerical model when it is used for simulating practical FWM devices. Also, two-photon absorption and the Kerr effect have negligible effects on interferometric converters and on SOAs used as in-line repeaters or preamplifiers, so we believe that neglecting them does not significantly limit the generality of the simulator.

B. Two-Pump FWM with Orthogonal Polarization

We compare in Fig. 5 the calculated and experimental spectra at the device output. The experimental results refer to an FWM

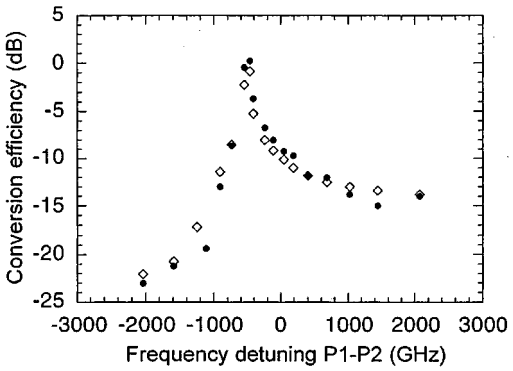

Fig. 6. Conversion efficiency versus frequency detuning between two CW pumps with the same polarization. Diamonds represent the results of the simulation whereas dots represent experimental results. The frequency detuning between the signal and one of the two pumps is fixed at 500 GHz, and the frequency of the signal is higher than the frequency of the pump.

experiment using two pumps of orthogonal polarization [24]. Even the higher order mixing contributions between the two pumps and the weak signal that appear in the experiment are well reproduced by the simulation. In addition, the simulation also shows mixing products covered by the ASE noise in the experiment and, therefore, not detectable.

C. Two-Pump FWM with Parallel Polarization

We simulated an FWM experiment using two pumps with parallel polarization, to check the ability of the simulator to reproduce the effects of the interference between the two pumps. In Fig. 6, we report the conversion efficiency versus the frequency detuning between two pumps with parallel polarization. Dots represent the results of an experiment. The experiment was performed for frequency down-conversion keeping the frequency detuning between one of the two pumps and the signal fixed to 500 GHz. Diamonds represent the results of simulations under the same conditions. The good agreement shown is an indication of the ability of the simulator to correctly account for the interference effects.

D. Evaluation of the Performance of an Optical System

To estimate the signal degradation due to ASE noise, we simulated the conversion of a single channel by calculating, with ASE noise, the eye diagrams after direct detection and comparing to the case in which ASE noise is switched off. The eye diagrams were obtained by detection of a binary sequence at $R = 10$ Gb/s represented by raised-cosine waveforms in the nonreturn to zero format. After detection, we used a third-order Butterworth filter of 0.4 R bandwidth. A quantitative estimate of the signal degradation was obtained by an approximate calculation of the BER based on a statistical analysis of the signal traces of the eye diagram, assuming all possible sequences of 3 bit. The case shown in Fig. 7 corresponds to an estimated BER of $2{\cdot}10^{-9}$, using optimal decision threshold and sampling time.

More complex transmission systems may also be simulated and the information obtained is potentially very valuable for experimentalists. We are working on the simulation of the mid-span spectral inversion scheme reported in [25], following the same approach described above for the evaluation of the BER.

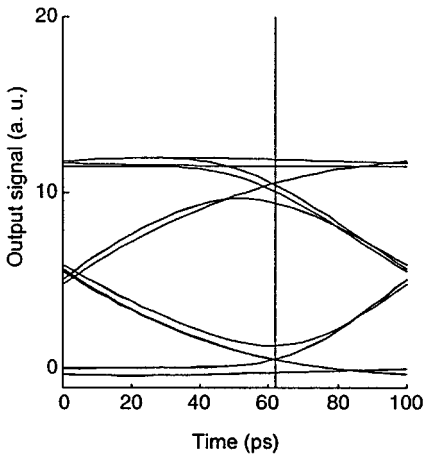

(a)

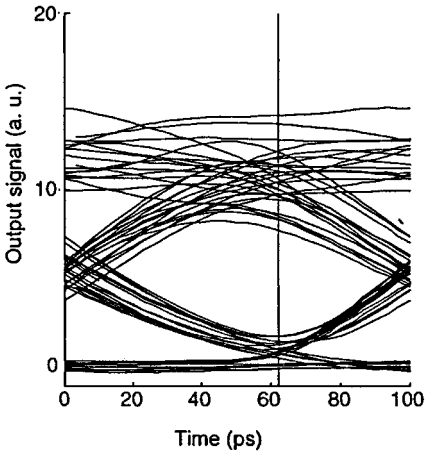

(b)

Fig. 7. Simulated eye diagrams obtained (a) without and (b) with ASE noise.

VI. CONCLUSIONS

We have described the essential steps of the derivation of an efficient numerical model of SOAs. We have validated our numerical model by comparing with the results of FWM experiments and showing good agreement. Although we have reported only simulations of FWM experiments, the model is indeed more general. It is suitable for investigating and predicting the performance of SOAs used as in-line amplifiers in single-channel and WDM transmission, where the amplifier saturation needs to be minimized to reduce the effect of crosstalk and intersymbol interference. The model can also simulate cross-gain and cross-phase modulation converters. The SOA simulator allows us to investigate separately the effect of different processes by switching on and off the analyzed process. The separation of the effect of ASE noise from the effect of nonlinear distortion shown in the paper is an example of this procedure.

Although the described numerical model gives an accurate description of the device, including propagation effects especially important when SOAs operate under saturation, it does not require long computational times, because it is based on the solution of a set of ordinary differential equations. Furthermore, since the device description is based on input–output relations, the simulator is ready to be inserted into more general modular

simulators of optical transmission systems. These features make the numerical model developed a useful tool for the optimization and evaluation of the performance of SOAs inserted into a real transmission systems.

ACKNOWLEDGMENT

The authors acknowledge useful discussions with J. Mørk, Technical University of Denmark, and P. Spano and B. Daino, Fondazione Ugo Bordoni. They would also like to thank A. D'Ottavi and F. Martelli, Fondazione Ugo Bordoni, as well as the laboratory group for supplying experimental data.

REFERENCES

[1] R. Castelli and T. Krause, "Market trends and evolution for optical transmission systems," *Alcatel Telecommun. Rev.*, 3rd Quarter 1998.

[2] V. W. S. Chan, K. L. Hall, E. Modiano, and K. A. Rauschenbach, "Architectures and technologies for high-speed optical data networks," *J. Ligthwave Technol.*, vol. 16, pp. 2146–2168, 1998.

[3] E. Iannone and R. Sabella, "Optical path technologies: A comparison among different cross-connect architectures," *J. Lightwave Technology*, vol. 14, pp. 2184–2196, 1996.

[4] E. Desurvire, *Erbium Doped Amplifiers-Principles and Applications*. New York, NY: Wiley, 1994.

[5] F. Brillouet, F. Devaux, and M. Renaud, "From transmission to processing: Challenges for new optoelectronic devices," *Alcatel Telecommun. Rev.*, 3rd Quarter 1998.

[6] Y. Maeno, Y. Suemura, A. Tajima, and N. Henmi, "A 2.56 Tb/s multiwavelength and scalable switch-fabric for fast packet-switching networks," *IEEE Photon. Technol. Lett.*, vol. 10, pp. 1180–1182, 1998.

[7] D. Nesset, M. C. Tatham, L. D. Westbrook, and D. Cotter, "Degenerate wavelength operation of an ultrafast all-optical AND gate using four-wave mixing in a semiconductor laser amplifier," *Electron. Lett.*, vol. 30, pp. 1938–1940, 1993.

[8] S. Kawanishi, "Ultrahigh-speed optical time-division-multiplexed transmission technology based on optical signal processing," *IEEE J. Quantum Electron.*, vol. 34, pp. 2064–2079, 1998.

[9] O. Katanami, S. Kawanishi, and M. Saruwatari, "Prescaled 6.3 GHz clock recovery from 50 Gbit/s TDM optical signal with 50 GHz PLL using four-wave mixing in a TWL optical amplifier," *Electron. Lett.*, vol. 30, pp. 807–809, 1994.

[10] A. Mecozzi and J. Mørk, "Saturation effects in nondegenerate four-wave mixing between short optical pulses in semiconductor laser amplifiers," *IEEE J. Select. Topics Quantum Electron.*, vol. 3, pp. 1190–1207, 1997.

[11] A. D'Ottavi, E. Iannone, A. Mecozzi, S. Scotti, P. Spano, J. Landreau, A. Ougazzaden, and J. C. Bouley, "Investigation of carrier heating and spectral hole burning in semiconductor amplifiers by nondegenerate four-wave mixing," *Appl. Phys. Lett.*, vol. 64, pp. 2492–2494, 1994.

[12] J. Mørk and A. Mecozzi, "Theory of the ultrafast optical response of active semiconductor waveguides," *J. Opt. Soc. Amer. B*, vol. 13, pp. 1803–1816, 1996.

[13] J. Mørk and J. Mark, "Time resolved spectroscopy of semiconductor laser devices: Experimentals and modeling," *Proc. SPIE*, vol. 2399, pp. 146–159, 1995.

[14] J. Mark and J. Mørk, "Subpicosecond gain dynamics in InGaAsP optical amplifiers: Experiments and theory," *Appl. Phys. Lett.*, vol. 61, pp. 2281–2283, 1992.

[15] K. Hall, G. Lenz, A. M. Darwish, and E. P. Ippen, "Subpicosecond gain and index nonlinearities in InGaAsP diode laser," *Opt. Commun.*, vol. 111, pp. 589–612, 1994.

[16] A. D'Ottavi, F. Girardin, L. Graziani, F. Martelli, P. Spano, A. Mecozzi, S. Scotti, R. Dall'Ara, J. Eckner, and G. Guekos, "Four-wave mixing in semiconductor optical amplifiers: A practical tool for wavelength conversion," *IEEE J. Select. Topics Quantum Electron.*, vol. 3, pp. 522–528, 1997.

[17] G. Contestabile, F. Martelli, A. Mecozzi, L. Graziani, A. D'Ottavi, P. Spano, G. Guekos, R. Dall'Ara, and J. Eckner, "Efficiency flattening and equalization of frequency up- and down-conversion using four-wave mixing in semiconductor optical amplifiers," *IEEE Photon. Technol. Lett.*, vol. 10, pp. 1398–1400, 1998.

[18] G. Hunziker, R. Paiella, D. F. Geraghty, K. J. Vahala, and U. Koren, "Polarization-independent wavelength conversion at 2.5 Gb/s by dual-pump four-wave mixing in a strained semiconductor optical amplifier," *IEEE Photon. Technol. Lett.*, vol. 8, pp. 1633–1635, 1996.

[19] A. Mecozzi, "Analytical theory of four-wave mixing in semiconductor amplifiers," *Opt. Lett.*, vol. 19, pp. 892–894, 1994.

[20] A. Mecozzi, S. Scotti, A. D'Ottavi, E. Iannone, and P. Spano, "Four-wave mixing in traveling-wave semiconductor amplifiers," *IEEE J. Quantum Electron.*, vol. 31, pp. 689–699, 1995.

[21] G. Guekos, Ed., *Photonic Devices for Telecommunications*. Berlin , Germany: Springer-Verlag, 1999.

[22] Y. Sun, A. K. Srivastava, S. Banerjee, J. W. Sulhoff, R. Pan, K. Kantor, R. M. Jopson, and A. R. Chraplyvy, "Error-free transmission of 32 × 25 Gb/s DWDM channels over 125 km of AllWave™ fiber using in-line semiconductor optical amplifiers," in *10th Optical Amplifiers and Their Applications*, Nara, Japan, June 9–11, 1999.

[23] Y. Sun, A. K. Srivastava, S. Banerjee, J. W. Sulhoff, R. Pan, K. Kantor, R. M. Jopson, and A. R. Chraplyvy, "Error-free transmission of 32 × 25 Gb/s DWDM channels over 125 km of AllWave™ fiber using in-line semiconductor optical amplifiers," in *OSA Tech. Dig.*, 1999, post-deadline paper PdP6.

[24] A. Mecozzi, G. Contestabile, F. Martelli, L. Graziani, A. D'Ottavi, P. Spano, R. Dall'Ara, J. Eckner, F. Girardin, and G. Guekos, "Optical spectral inversion without frequency shift by four-wave mixing using two pumps with orthogonal polarizations," *IEEE Photon. Technol. Lett*, vol. 10, pp. 335–337, 1998.

[25] A. Corchia, C. Antonini, A. D'Ottavi, A. Mecozzi, F. Martelli, P. Spano, G. Guekos, and R. Dall'Ara, "Mid-span spectral inversion without frequency shift for fiber dispersion compensation: A system demonstration," *IEEE Photon. Technol. Lett*, vol. 11, pp. 275–277, 1999.

Dajana Cassioli was born in Rome, Italy, on August 29, 1971. She received the "laurea" degree in electrical engineering from the University of Rome II "Tor Vergata," Rome, Italy, in 1999. Her thesis was on the study of the optical nonlinearity of semiconductor optical amplifiers and on the computer simulation of devices based on semiconductor optical amplifiers in WDM optical transmission systems.

She is presently involved at the Fondazione Ugo Bordoni, Rome, Italy, on the realization of a computer simulator of optical transmission systems.

Simona Scotti was born in Rome, Italy, on April 28, 1956. She received the laurea degree in physics from "La Sapienza" University of Rome in 1980.

She was at Fondazione Ugo Bordoni, Rome, Italy, in 1981 during a scholarship carrying out studies on automatic speaker recognition. Since 1983, she has been a Researcher in the Optical Communication Division of Fondazione Ugo Bordoni, where she has been involved in experimental characterization and modeling of optical passive devices. Her current interest is in the field of active semiconductor devices, with special aim at studying nonlinear effects in semiconductor optical amplifiers used in communication systems.

Antonio Mecozzi (M'97) received the laurea degree in chemical engineering from the University of Rome, Rome, Italy, in 1983.

From 1985 to 1999, he was with the Optical Communication Division of Fondazione Ugo Bordoni, Rome, Italy, with the exception of a period spent at the Research Laboratory of Electronics of MIT from 1991 to 1992. Since November 1999, he has been an Associate Professor of Structure of Matter at the University of L'Aquila (Italy). His main research interests are quantum electronics and optical fiber communications.

Dr. Mecozzi is a member of the IEEE Lasers and Electro-Optics Society and a fellow of the Optical Society of America.